Gas-phase transport of WF_6 through annular nanopipes in TiN during chemical vapor deposition of W on TiN/Ti/SiO_2 structures for integrated circuit fabrication

G. Ramanath,[a] J. R. A. Carlsson, J. E. Greene, and L. H. Allen
Coordinated Science Laboratory, Materials Research Laboratory, and Department of Materials Science, University of Illinois, 1304 W. Green Street, Urbana, Illinois 61801

V. C. Hornback and D. J. Allman
Symbios Logic Inc., 1635 Aeroplaza Drive, Colorado Springs, Colorado 80916

(Received 2 August 1996; accepted for publication 6 September 1996)

Delamination of TiN/Ti bilayers on SiO_2 is a serious problem during W chemical vapor deposition (CVD) using WF_6 to form vertical interconnects in integrated circuits. In order to obtain insight into the delamination mechanism, we have determined depth-distributions of W and F in sputter-deposited TiN/Ti bilayers on SiO_2 as a function of WF_6 exposure time t_{WF_6} at 445 °C. Even for $t_{WF_6}<6$ s, significant concentrations of both W ($\approx$3.5 at. %) and F ($\approx$2 at. %) penetrate through the 106-nm-thick TiN film. W piles up at the TiN/Ti interface, while F rapidly saturates the TiN layer and accumulates in the Ti underlayer at concentrations up to $\approx$10 at. % for $t_{WF_6}=60$ s. Cross-sectional and scanning transmission electron microscopy analyses demonstrate that WF_6 penetrates into the TiN layer through nanometer-scale intercolumnar voids spanning the entire film thickness and reacts with the Ti underlayer. We propose that the high F concentrations in the Ti layer weakens the Ti/SiO_2 interface leading to adhesion failure of the TiN/Ti bilayer. © *1996 American Institute of Physics.* [S0003-6951(96)00247-1]

Chemical vapor deposition (CVD) of W from WF_6 is used to fill small contact holes and vias for connecting adjacent metallization layers in ULSI device fabrication.[1] CVD W exhibits high electrical conductivity with good step coverage at high aspect ratio features and has a relatively low deposition temperature.[2,3] The W vertical interconnects are usually deposited on thin TiN/Ti bilayer liners, in which TiN (typically 50–100 nm thick) serves as a low contact-resistance diffusion barrier and Ti ($\approx$30 nm) enhances the adhesion between TiN and the underlying Si or SiO_2.[1]

A serious problem with sputter-deposited TiN/Ti liners is their delamination around vias and contacts during the early stages of W CVD.[4–6] Current short term solutions involve additional processing steps such as a rapid thermal anneal at temperatures $\geqslant$650 °C prior to W CVD on contacts, and the use of thicker TiN layers. However, the mechanisms leading to delamination are still not understood. The continuing reduction in device dimensions and the associated use of high aspect ratio vias is unexpected to exacerbate the adhesion problem owing to poor conformality of sputter-deposited TiN/Ti liners at via sidewalls and stress concentration at via corners. In this letter, we report the results of initial experiments designed to identify the primary adhesion-failure mechanisms.

The substrates used in this study were 700-nm-thick SiO_2 layers deposited by plasma enhanced CVD on 200-mm-diam Si(100) wafers. Thin films of Ti (27 nm) and TiN (106 nm) were sequentially deposited at 250 °C, without breaking vacuum, by reactive magnetron sputtering in an Applied Materials Endura HP process tool. The base pressure in the deposition chamber was 1×10^{-8} Torr and sputtering was carried out in pure Ar for Ti deposition and a 3:6:1 N_2:Ar mixture for TiN. The total pressure was 5 mTorr in both cases yielding deposition rates of 2.2 and 1.8 nm s^{-1} for Ti and TiN, respectively. A Novellus Systems Concept One cold-wall CVD reactor was used for the WF_6 exposures which were carried out at 445 °C in a 30:1 Ar:WF_6 mixture at a flow rate of 1.2 ℓ min^{-1} and a total pressure of 40 Torr.

TiN film compositions were determined by Rutherford backscattering spectroscopy (RBS) and the spectra were analyzed through comparisons with RUMP[7] computer simulations. The RBS probe beam consisted of 2 MeV $^4He^+$ ions incident at angles between $-10°$ and 30° to the sample normal and the detector was set at a scattering angle of 150°. N/Ti ratios in the TiN films were found to be 1.01 ± 0.02. Compositional depth profiles through the bilayer samples before and after WF_6 exposures were determined by RBS and secondary ion mass spectrometry (SIMS). The SIMS measurements were performed in a Cameca IMS 5f instrument with an 8 keV O_2^+ primary beam. W and F concentrations were estimated based upon established relative sensitivity factors in TiN and Ti matrices.[8]

The microstructure of the TiN/Ti bilayers was characterized by plan-view and cross-sectional transmission electron microscopy (TEM and XTEM) in a Philips CM12 microscope operated at 120 kV. Z-contrast imaging of cross-sectional specimens was performed in a Vacuum Generators HB501 scanning TEM (STEM) at 100 kV with a 1-nm-diam electron beam in order to determine local changes in film microchemistry upon WF_6 exposure. A combination of RBS and TEM showed that the TiN layers were underdense, while Ti layers exhibited essentially bulk density.

Typical W SIMS depth profiles from an as-deposited TiN/Ti sample and samples exposed to WF_6 for times t_{WF_6} between 6 and 60 s are reproduced in Fig. 1(a). W penetrates

[a] Electronic mail: ramanath@uiuc.edu

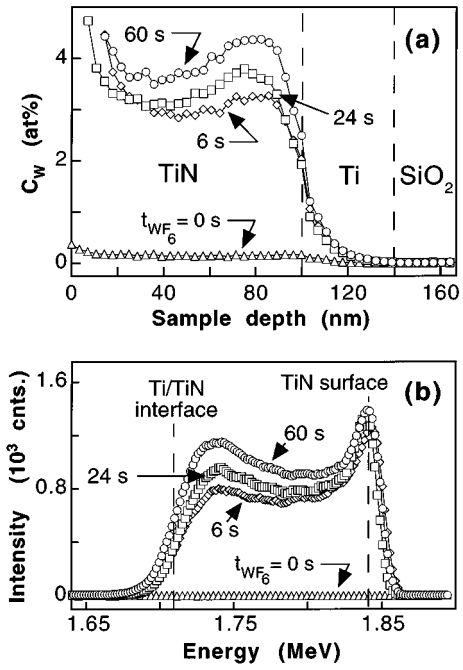

FIG. 1. Representative (a) SIMS and (b) RBS depth profiles of W in TiN/Ti/SiO_2 following exposure to WF_6 at 445 °C for times t_{WF_6} ranging from 0 to 60 s. The dashed vertical lines show approximate positions of the TiN surface and the TiN/Ti interface.

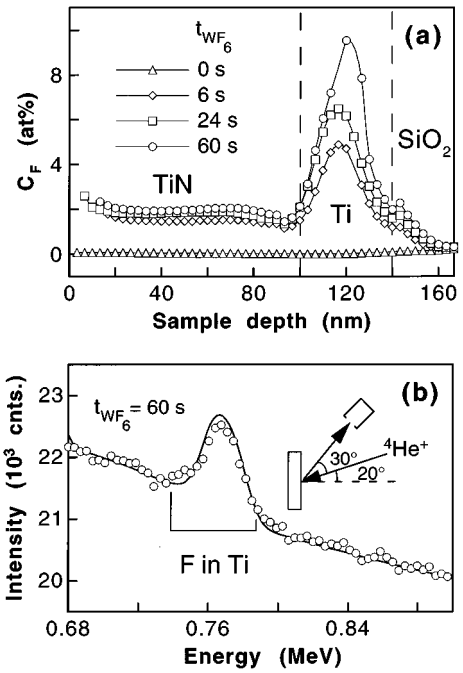

FIG. 2. (a) Representative SIMS depth profiles of F in TiN/Ti/SiO_2 exposed to WF_6 following exposure to WF_6 at 445 °C for times t_{WF_6} ranging from 0 to 60 s. (b) The F-in-Ti portion of a RBS spectrum from a sample exposed to WF_6 for $t_{WF_6}=60$ s. The solid curve is a simulated spectrum.

the entire depth of the TiN film in <6 s and begins to accumulate near the TiN/Ti interface. While the W concentration C_W in the bulk of the TiN film increases slightly from ≈ 3 at. % at $t_{WF_6}=6$ s to 3.5 at. % at $t_{WF_6}=60$ s, W accumulation at the interface increases more rapidly, from ≈ 3 to 4.5 at. % for the same WF_6 exposure times. The penetration of W into the Ti layer is negligible, <0.1 at. % even at the WF_6 highest exposure, due to both low solubility[9] and a sluggish diffusion rate. Thus, W piles up at the TiN/Ti interface.

The RBS spectra and RUMP simulations in Fig. 1(b) confirm the W accumulation at the TiN/Ti interface shown by SIMS analysis and indicate that the maximum nominal thickness of W deposited on the top TiN surface is ≈ 2 ML.

In contrast, the SIMS profiles in Fig. 2(a) show that while F also penetrates the TiN layer upon WF_6 exposure, there is no measurable tendency for F accumulation at the TiN/Ti interface. In fact, F continues to migrate and penetrates the entire Ti underlayer. From the profiles, a lower bound for the diffusivity of F in polycrystalline Ti at 445 °C was estimated to be $\approx 10^{-12}$ cm^2 s^{-1}. The F concentration C_F in the TiN layer reaches a saturation value of ≈ 2 at. % at WF_6 exposures less than the lowest value used in our experiments, $t_{WF_6}=6$ s. However, C_F in the Ti layer continues to increase with the maximum value ranging from ≈ 5 at. % for $t_{WF_6}=6$ s to ≈ 9.5 at. % at $t_{WF_6}=60$ s.

The RBS spectra are consistent with the SIMS profiles showing a buildup of F in the Ti layer. From fitting experimental data with simulated spectra [see Fig. 2(b)] and assuming bulk Ti density, the total F content in Ti is ≈ 10 at. % for $t_{WF_6}=60$ s, in good agreement with SIMS analyses. The simulated spectra also suggest that F accumulates near the Ti/SiO_2 interface.

The penetration depths of W and F in TiN are several orders of magnitude larger than can be explained by bulk solid-state diffusion at the temperatures used in our experiments.[3] The results can be understood, however, based upon TEM and XTEM analyses showing that the TiN film is underdense with a porous microstructure. Figure 3(a) is a typical plan-view TEM micrograph revealing TiN grains of average size 15 ± 4 nm separated by annular intercolumnar voids having a mean width of 1.3 ± 0.3 nm. The absence of Moiré fringes indicates that the TiN grains are columnar as confirmed by XTEM micrographs which showed that the void network spans the entire thickness of the TiN layer. This microstructure is typical of reactively sputter-deposited polycrystalline TiN and $Ti_{0.5}Al_{0.5}N$ films grown at low temperatures, <500 °C, where cation surface mobilities are low.[10,11] XTEM analyses showed that the Ti layers were dense with nearly equiaxed grains of average diameter 25 ± 2 nm.

The open intercolumnar voids in the TiN film act as nanometer-scale annular diffusion pipes allowing gas-phase transport of the relatively small WF_6 molecules (diameter $=0.36$ nm[12]) to exposed Ti surface regions at the TiN/Ti interface. Moreover, the nanopipes provide internal TiN surfaces for dissociative WF_6 adsorption and dissociation leading to the deposition of W and F along the walls of the nanopipes. Thus, W serves as a marker highlighting WF_6 diffusion paths. This is clearly seen in the Z-contrast[13] STEM micrograph in Fig. 3(b). Since the contrast arises from the Z^2 dependence of the high-angle (>40 mrad) scattered electron intensity, the heavier W atoms appear bright in the TiN matrix. This was confirmed in the STEM by elemental mapping of XTEM specimens using energy dispersive x-ray spectroscopy.

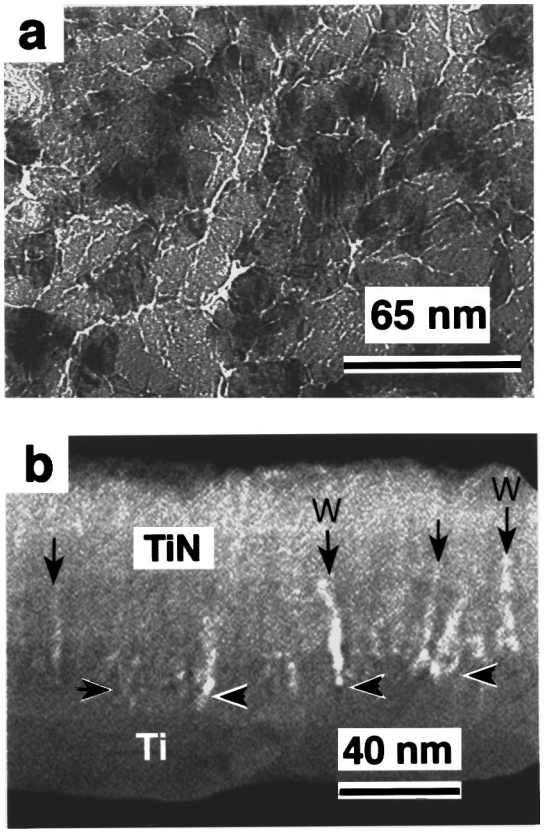

FIG. 3. (a) Bright field plan-view TEM micrograph of the TiN layer showing the network of nanometer-scale voids (white regions) surrounding columnar grains. (b) Dark-field cross-sectional *Z*-contrast STEM image of a $TiN/Ti/SiO_2$ structure following WF_6 exposure at 445 °C for $t_{WF_6}=60$ s. The vertical arrows point to W (bright regions) deposited along intercolumnar voids in the TiN film while the horizontal arrows point to regions of W accumulation at the TiN/Ti interface.

Our experiments involving WF_6 exposure in the absence of gas-phase reducing agents such as H_2 or SiH_4 simulate the early stages of W CVD on TiN/Ti bilayers, prior to the formation of a continuous W layer, in which the TiN and Ti surfaces themselves act as reductants. WF_6 molecules are incident on the TiN surface and the top of the annular nanopipes at angles varying over 2π sterad. W deposition in the pipes is initiated, on average, near the top. However, the reactive sticking probability of WF_6 is lower on W than on TiN.[3] Thus, as W deposition proceeds down the walls of the nanopipes, subsequently entering WF_6, molecules must undergo an increased number of wall collisions before they are dissociatively adsorbed. This results in a decrease in the overall WF_6 reaction rate which, together with the pinching off of the nanopipes due to W deposition, causes the W concentration in TiN to saturate.

Fluorine is also deposited along the TiN nanopipes. However, our results show that $C_F < C_W$ and that C_F saturates very rapidly. This implies that during W and F deposition, excess F is rejected from the TiN nanopipes by the evolution of volatile products including TiF_4, WF_x, and F_2.[3] F_2 and WF_x, together with WF_6, transport F along the nanopipes to the exposed surface of the Ti underlayer where their reduction is expected to be facile. WF_6, for example, is much more reactive with Ti (leading to TiF_3 formation even at room temperature) than with TiN.[2] W deposition on the exposed Ti surface impedes further WF_x reduction and acts as a barrier to additional F injection into Ti. However, the fact that the F concentration in Ti continues to increase significantly with increasing WF_6 exposure indicates that W coverage on exposed Ti film surfaces is incomplete even for the largest t_{WF_6} values used in our experiments. Thus, the remaining exposed Ti still serves as a sink for F arriving by surface diffusion along the nanopipes. The extremely small Ti exposed surface area to volume ratio at the bottom of the nanopipes inhibits F buildup at the Ti surface by enhancing the migration of F through the Ti layer to the Ti/SiO_2 interface. We believe that F-induced weakening of the Ti/SiO_2 interface is the primary cause of TiN/Ti bilayer delamination.

In summary, we have demonstrated that large concentrations of W and F enter the sputter-deposited TiN ''diffusion barrier'' layer during the early stages of W CVD from WF_6. A network of intercolumnar voids spanning the entire thickness of the TiN layer allows WF_6 and other F-containing reaction products to reach and react with exposed surface regions of the Ti underlayer. While W accumulates at the TiN/Ti interface, F rapidly diffuses through the Ti layer to the Ti/SiO_2 interface, leading to adhesion failure.

We gratefully acknowledge financial support from the Joint Services Electronics Program and the Materials Science Division of the U.S. Department of Energy under Contract No. DEAC0276ER01198. We also appreciate useful discussions with Dr. J. Baker and thank Ms. M. Mochel for assistance with STEM measurements. Microanalysis and surface analysis were performed at the Center for Microanalysis of Materials, University of Illinois, funded by the Department of Energy.

[1] See, for example, short review articles in the Mater Res. Soc. Bull. (1995), and references therein.
[2] M. L. Yu, Y. Ahn, and R. V. Joshi, J. Appl. Phys. **67**, 1055 (1990); IBM J. Res. Dev. **36**, 875 (1990), and references therein.
[3] S. L. Lantz, A. E. Bell, W. K. Ford, and D. Danielson, J. Vac. Sci. Technol. A **12**, 1032 (1994), and references therein.
[4] M. M. Farahani, J. F. Buller, B. T. Moore, and S. Garg, IEEE Trans. Semicond. Manuf. **7**, 79 (1994).
[5] M. Rutten, D. Greenwell, S. Luce, and R. Dreves, *Advanced Metallization for ULSI Applications*, edited by V. V. S. Rana, R. V. Joshi, and I. Ohdomari (Materials Research Society, Pittsburgh, PA, 1992), p. 277.
[6] G. Ramanath, V. C. Hornback, D. J. Allman, J. R. A. Carlsson, and L. H. Allen, Proceedings of the 13th International VLSI Mult. Interconn. Conference, Santa Clara, CA, 1996, p. 333.
[7] L. R. Doolittle, Nucl. Instrum. Methods Phys. Res. B **9**, 334 (1985); *ibid.* **15**, 227 (1986); also see *Genplot Manual* (Computer Graphics Service, New York, 1990).
[8] G. E. Lux, F. A. Stevie, P. M. Kahora, R. G. Wilson, and G. W. Cochran, J. Vac. Sci. Technol. A **11**, 2373 (1993); R. G. Wilson (private communication).
[9] *Phase Diagrams of Binary Titanium Alloys*, edited by J. L. Murray (ASM, Metals Park, OH, 1987), p. 328.
[10] I. Petrov, L. Hultman, U. Helmersson, J.-E. Sundgren, and J. E. Greene, Thin Solid Films **169**, 299 (1989).
[11] F. Adibi, I. Petrov, J. E. Greene, L. Hultman, and J.-E. Sundgren, J. Appl. Phys. **73**, 8580 (1993).
[12] *JANAF Thermochemical Tables*, edited by W. W. Chase, C. A. Davies, J. R. Downey, D. J. Frurip, R. A. McDonald, and A. N. Syverud (National Bureau of Standards, Washington, DC, 1985).
[13] For a recent review, see, S. J. Pennycook, D. E. Jesson, M. F. Chisholm, N. D. Browning, A. J. McGibbon, and M. M. McGibbon, J. Microsc. Soc. Am. **1**, 231 (1995).